Optical Materials 33 (2011) 543–548

Contents lists available at ScienceDirect

Optical Materials

journal homepage: www.elsevier.com/locate/optmat

The gain and noise figure of Yb–Er-codoped fiber amplifiers based on the temperature-dependent model

Abdel Hakeim M. Husein [a,*], Ali H. El-Astal [a], Fady I. EL-Nahal [b]

[a] Department of Physics, Al-Aqsa University, P.O. Box 4051, Gaza, Gaza Strip, Palestine
[b] Department of Elec. Eng., Islamic University of Gaza, Gaza, Palestine

ARTICLE INFO

Article history:
Received 12 April 2010
Received in revised form 26 October 2010
Accepted 27 October 2010
Available online 26 November 2010

Keywords:
Optical fiber
EDFA
YDFA
Noise figure

ABSTRACT

A novel temperature-dependent model for Yb^{3+}–Er^{3+}-codoped fiber amplifier (EYDFA) based on the energy transfer from Yb^{3+} to Er^{3+} is established. Using appropriate fiber and energy transfer parameters, the coupled rate equations is numerically solved at 25 and 40 °C. The pumping powers are 100 and 200 mW at a pump wavelength of 1060 nm. The signal gain and noise characteristics of a 0.3 m erbium/ytterbium co-doped fiber (EYDF) in a single-pass configuration are investigated by using 1, 10 and 100 μW signals at 1535 nm. A maximum signal gain of 40.5 dB and a corresponding noise figure of 3.65 dB at the temperature of 25 °C are achieved.

1. Introduction

Erbium doped fiber amplifiers (EDFAs) have been widely deployed for long-haul fiber communication systems [1]. The fabrication of a short-length and high-gain optical amplifier, operating around 1550 nm is of a great interest. It needs optical mediums doping with high concentration of erbium, where the main problem is the reduction of gain and pump efficiency due to the concentration quenching. Short amplifiers (∼ a few cm long) with high-gain are also vital in communication networks where latency is crucial. High gain (>10 dB) in short-length amplifiers can be achieved by using high concentration of erbium. On the other hand the ion–ion interactions which causes pair-induced up-conversion depletes the erbium meta-stable level and lowers the pump efficiency for concentration above a few hundred parts per million (ppm) of Er [2]. Currently, investigating the gain performance of erbium-doped fiber amplifiers is attracting much attention [3–8].

This issue has been addressed by co-doping the Er-doped fiber with Yb [9–11]. The presence of Yb reduces the formation of Er clusters and reduces the up-conversion rate from the upper level of Er ($^4I_{13/2}$ level) significantly. This allows high erbium doping level needed for a high gain amplifier. Moreover, an efficient indirect pumping mechanism of Er ions is provided by an energy transfer from Yb to Er. This energy transfer mechanism is very efficient and thus for an Er–Yb-codoped amplifier the preferred pump wavelength corresponds to an Yb transition. In this scheme, the $^2F_{5/2}$ level of Yb^{3+} ions is close to the Er $^4I_{11/2}$ and $^4I_{9/2}$ manifolds. Then involvement of 1–2 phonons can make energy transfer between these two states possible. Besides, if a pair of two excited Yb^{3+} ions is formed (with the energy of about 20,000 cm^{-1}), it can be also transferred to the $^4F_{7/2}$ and $^2H_{11/2}$ states of Er^{3+}, with a subsequent Er^{3+} emission. The dynamics of Er^{3+} emission depends on both Er^{3+} and Yb^{3+} concentrations as well as the optical properties of the host. The upconversion of Er^{3+} ions is influenced by the multiphonon relaxation. The multiphonon relaxation probability depends mainly on the energy gap between two successive levels and the phonon energy of the host. The nonradiative decline of the excited electronic states of rare-earth ions in solids is controlled by the highest energy phonons. When these vibrations are characterized by high frequencies, this affects the upconversion process as the ion relaxes via the emission of phonons rather than photons. The multiphonon relaxation rates are vital in determining the upconversion efficiency. This indirectly affects the gain and introduces loss in the fiber [12]. EYDFAs have many practical benefits such as a wide pump absorption band, which enables an extended range of pump laser wavelengths. In an EYDFA, energy transfer from the excited states of Yb to that of Er is used to form a population inversion between lasing levels of Er. Fig. 1 shows the absorption spectrum of Er/Yb co-doped fiber system [13]. It is clear from the figure, the pump wavelength for Er-doped fiber is near the 980 nm whereas the ytterbium–erbium ions are pumped at the absorption wavelength of 800–1100 nm. In this work 1060 nm pump wavelength has been used because the Yb^{3+} has very broad absorption spectrum allowing a verity of pumping scheme to generate gain at longer wavelength [14,15].

* Corresponding authors.
E-mail addresses: hakeim00@alaqsa.edu.ps (A.H.M. Husein), a_elastal@alaqsa.edu.ps (A.H. El-Astal), fnahal@iugaza.edu.ps (F.I. EL-Nahal).

0925-3467/$ - see front matter © 2010 Elsevier B.V. All rights reserved.
doi:10.1016/j.optmat.2010.10.050

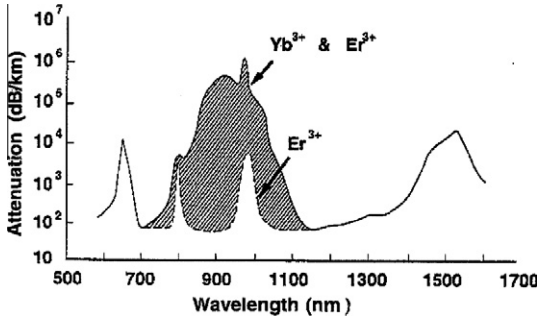

Fig. 1. The absorption spectrum of the Er^{3+}/Yb^{3+} co-doped fiber along with the spectrum of the erbium ions for comparison [13].

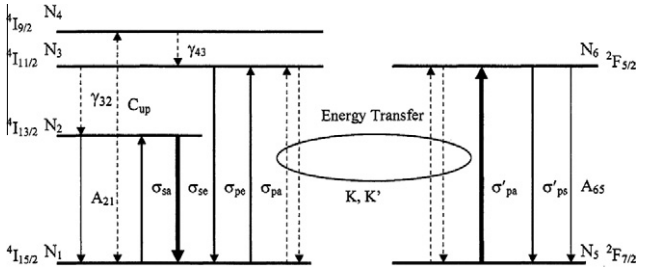

Fig. 2. Energy level diagram of (a) Er (erbium) and (b) Yb (ytterbium) systems. The dashed lines and the solid lines represent non-radiative and radiative transitions, respectively.

A high concentration of Yb^{3+} is needed for efficient pumping of the Er/Yb co-doped fiber amplifier (EYDFA) system which has a reduced sensitivity to pump power fluctuation. Appropriate theoretical and computational algorithms play a key role in predicting amplifier performances and yielding improved device designs. On the other hand, the accuracy of the results depends not only on the numerical models, but also on the characteristic parameters involved in the models such as the temperature which is an important parameter for the accuracy.

Here we present the temperature-dependent model and numerical results of the gain (G) and noise figure (NF) at the signal wavelength of 1535 nm for Er–Yb amplifiers (with a single mode core doped with both Er and Yb) at two different temperatures. The injected pump light also propagates in the fiber and absorbed in the core region for the amplification signal. The feasibility of Er–Yb co-doped single mode fiber amplifier that has a considerable gain (~40 dB) and short length (30 cm) has been shown.

2. Theoretical model

Er (erbium) and Yb (ytterbium) co-doped fibers act as four-level laser systems. The energy level schemes for these two ions (system) along with possible transitions are shown in Fig. 2. The transitions involve both radiative and non-radiative energy transfer processes. It also includes the up-conversion effects at the signal wavelength. This effect is not considered at the pump wavelength. Where the pump power is distributed in the cladding area, absorbed in the core region and has much smaller power density.

On the basis of the energy level diagram, the rate equations for Er and Yb population densities can be written as [16]:

$$\frac{dN_2}{dt} = -A_{21}N_2 - 2C_{up}N_2^2 + N_1\sigma_{sa}\phi_s - N_2\sigma_{se}\phi_s + \gamma_{32}N_3 \quad (1)$$

$$\frac{dN_3}{dt} = -N_3\sigma_{pe}\phi_p + N_1\sigma_{pa}\phi_p + KN_6N_1 - K'N_3N_5 - \gamma_{32}N_3 + \gamma_{43}N_4 \quad (2)$$

$$\frac{dN_4}{dt} = C_{up}N_2^2 - \gamma_{43}N_4 \quad (3)$$

$$N_1 + N_2 + N_3 + N_4 = N_{Er} \quad (4)$$

$$\frac{dN_5}{dt} = +KN_6N_1 - K'N_3N_5 - N_5\sigma'_{pa}\phi_p + N_6\sigma'_{pe}\phi_p + A_{65}N_6 \quad (5)$$

$$N_5 + N_6 = N_{Yb} \quad (6)$$

The parameters in the rate equations are as follows: The quantities N_1, N_2, N_3 and N_4 (m^{-3}) are the Er^{3+} population densities of the $^4I_{15/2}$, $^4I_{13/2}$, $^4I_{11/2}$, and $^4I_{9/2}$ levels, respectively. The quantities N_5 and N_6 (m^{-3}) are the Yb^{3+} population densities of the $^2F_{7/2}$ and $^2F_{5/2}$ levels, respectively. σ_{sa} and σ_{se} (m^2) are the absorption and emission cross sections of Er^{3+} at the signal wavelength, respectively. σ_{pa} and σ_{pe} (m^2) are the absorption and emission cross sections of Er^{3+} at the pump wavelength, respectively. σ'_{pa} and σ'_{pe} (m^2) are the absorption and emission cross-sections of Yb^{3+} at the pump wavelength. γ_{43} and γ_{32}(s^{-1}) are the non-radiative transition rates of Er^{3+}. A_{21} (s^{-1}) and A_{65} (s^{-1}) are the spontaneous emission rates of Er^{3+} and Yb^{3+}. C_{up} ($m^3\ s^{-1}$) is up-conversion coefficient from $^4I_{13/2}$ to $^4I_{9/2}$ level of Er^{3+}. This process cannot be neglected when the signal power is high, which is the case in this application. The energy transfer coefficients K and K' ($m^3\ s^{-1}$) are largely dependent of Er concentration. Furthermore, K also depends on the host glass. The quantities ϕ_p and ϕ_s ($m^{-2}\ s^{-1}$) are the pump and signal photon fluxes, respectively. In this model, Er^{3+} ions are assumed homogenously excited. This implies that they experience similar surroundings, that the up-conversion rate is homogenously. The ratio N_{Yb}/N_{Er} is chosen for efficient energy transfer and to avoid the formation of Er clusters. Therefore, Er concentration is large enough to allow rapid energy migration in the Er sub-system. The energy migration can be expected to be higher than the up-conversion rate due to the poor spectral overlap for the up-conversion process [17]. Thus, the up-conversion may saturate in the kinetic limit. Therefore, homogenous up-conversion is modeled by a relaxation term which is quadratic in the concentration of excited Er^{3+}, with a concentration independent up-conversion coefficient. We believe that this assumption is reasonable when Er^{3+} clusters are not present. However, if Yb^{3+} concentration is low, it will not prevent the formation of Er^{3+} clusters and they will act as quenching centers, where rapid up-conversion takes place thus causing inefficient energy transfer [18]. These quenching centers are extremely harmful in Er–Yb system, because the efficient pumping of quenching center will result in an efficient drain for the pump light [19]. From Eqs. ()()()(1)–(3), we obtain the following solution at steady state

$$N_4 = \frac{C_{up}N_2^2}{\gamma_{43}} \quad (7)$$

$$N_3 = \frac{A_{21}N_2 + 2C_{up}N_2^2 - N_1\sigma_{sa}\phi_s + N_2\sigma_{se}\phi_s}{\gamma_{32}} \quad (8)$$

The non-radiative relaxation rates γ_{32} and γ_{43} are about $10^9\ s^{-1}$ for the parameters used in the numerical calculations. Therefore, N_3 and N_4 are much smaller than N_1 and N_2. Hence $N_{Er} = N_1 + N_2$. The equation governing the population density of Er^{3+} and Yb^{3+} at $^4I_{11/2}$ and $^2F_{5/2}$, respectively, becomes as follows:

$$\frac{dN_2}{dt} = -A_{21}N_2 - C_{up}N_2^2 - N_2\sigma_{se}\phi_s + (N_{Er} - N_2)(\sigma_{sa}\phi_s + \sigma_{pa}\phi_p + KN_6) \quad (9)$$

$$\frac{dN_6}{dt} = -KN_6(N_{Er} - N_2) + (N_{Yb} - N_6)\sigma'_{pa}\phi_p - N_6\sigma'_{pe}\phi_p - A_{65}N_6 \quad (10)$$

In the lower signal power application (1–100 μW), the up-conversion process can be neglected because the cross-relaxation procedure dominants much more on the up-conversion process

[20]. In this study, the cross-relaxation coefficient, $K = 3 \times 10^{-20}\ m^3\ s^{-1}$, is much larger than the up-conversion coefficient, $C_{up} \cong 10^{-24}\ m^3\ s^{-1}$, and this therefore leads to simplify and avoid quadratic terms in Eq. (9). The solutions of N_2 and N_6 at steady state are;

$$N_2 = \frac{N_{Er}(\sigma_{sa}\phi_s + \sigma_{pa}\phi_p + KN_6)}{A + \sigma_{se}\phi_s + (\sigma_{sa}\phi_s + \sigma_{pa}\phi_p + KN_6)} \tag{11}$$

$$N_6 = \frac{\phi_p N_{Yb}\sigma'_{pa}}{\phi_p\sigma'_{pa} + \phi_p\sigma'_{pe} + A_{65} + K(N_{Er} - N_2)} \tag{12}$$

The propagation equation of ASE can be written as [16]

$$\frac{dP_{ASE_\pm}(z,\nu_j)}{dz} = \mp\alpha_s P_{ASE_\pm}(z,\nu_j) \pm [\sigma_{sa}(\nu_j)N_2 - \sigma_{se}(\nu_j)N_1]\Gamma_s P_{ASE_\pm}(z,\nu_j) \pm mh\nu_j\Delta\nu_j\sigma^{Er}_{sa}N_2\Gamma_s \tag{13}$$

where α_s is the propagation loss at signal wavelength, $\sigma^{Er}_{e12}(\nu_j)$ and $\sigma^{Er}_{a12}(\nu_j)$ represents the absorption and emission cross-section of Er^{3+} ions between levels i, j at centered frequency ν_j, m is the number of modes h Planck's constant, $\Delta\nu_j$ is the band width and Γ_s is the signal overlap factor.

In the presence of a crystal field, each atomic level is broadened into a band of energy levels. The energy in Quasi three laser level is shown in Fig. 3 which illustrates that there is rapid thermalization of levels within each manifold. Therefore the relative populations of levels within manifold can be treated by Boltzmann equilibrium. The rate equations of Quasi three level laser system include the Boltzmann factors as a function of temperature and that govern the pump process are [21]

$$\frac{dI^{\pm}(z,t)}{dz} = \mp(f'_aN_0 - f'_bN_1)\sigma_{ab}I^{\pm}(z,t) \tag{14}$$

$$\frac{dN_1(z,t)}{dt} = \sigma_{ab}(f'_aN_0 - f'_bN_1)\frac{I^{\pm}(z,t)}{h\upsilon_p} - \frac{N_1(z,t)}{\tau_f} \tag{15}$$

where N_0, N_1 and $N_t = N_0 + N_1$ are the lower manifold population density, upper manifold population density, and total doping density, respectively. The $f'_a$and f'_b are the Boltzmann occupation factor within lower and upper manifolds for the lower and upper levels of the pump transition. Similarly, for the laser transitions f_a and f_b are the Boltzmann occupation factors for lower and upper levels of the laser transition within the lower and upper manifolds, respectively. σ_{ab} is the spectroscopic absorption cross section at the pump wavelength, τ_f is the upper manifold lifetime, and $h\upsilon_p$ is the pump photon energy. $I^+(z,t)$ and $I^-(z,t)$ are the pump intensities propagating in the forward and backward directions, respectively. Here for explicitly allow the possibility that f'_b may not be zero which is the case for several solid-state laser systems such as Yb^{3+} pumped on the $^2F_{7/2} \rightarrow {}^2F_{5/2}$ transition, and Er^{3+} pumped on the $^4I_{15/2} \rightarrow {}^4I_{13/2}$ transition.

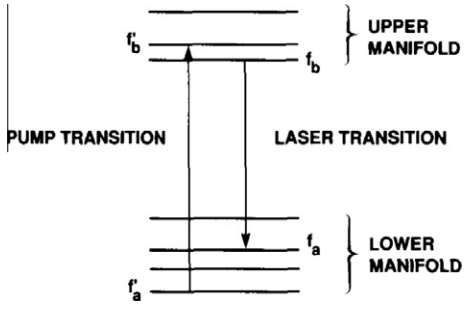

Fig. 3. The assumed energy level diagram showing the pump and laser transitions.

The Boltzmann distribution law gives the population distribution of the atoms in a band and the calculation of Boltzmann factors can be done through Spark level splitting [21,22]:

$$N_a = \frac{N_0}{Z_a}\exp(-E_a/kT) = f_aN_0 \quad \text{and}$$

$$Z_a = \sum_i^4 \exp(-E_i/kT) \quad \text{for Yb ground state} \tag{16}$$

$$N_b = \frac{N_1}{Z_b}\exp(-E_b/kT) = f_bN_1 \quad \text{and}$$

$$Z_b = \sum_i^3 \exp(-E_i/kT) \quad \text{for Yb excited state} \tag{17}$$

where N_a is the lower band of the population density of the energy level E_a, N_0 is the population density of the lower level and T is the temperature in celsius, so $N_a = f_aN_0$. For the upper level population, N_b is given by $N_b = f_bN_1$, where N_1 is the upper manifold population. Similarly, for the pump transitions $N'_a = f'_aN_0$ and $N'_b = f'_bN_1$. All Boltzmann factors in Eqs. (16) and (17) as function of temperature due to the thermalization between each manifolds. By including these Boltzmann factors in the population, the N_6 equation becomes:

$$N_6 = \frac{\phi_p N_{Yb}\sigma'_{pa}f'_a}{\phi_p\sigma'_{pa}f'_a + \phi_p\sigma'_{pe}f'_b + A_{65} + K(N_{Er} - N_2)} \tag{18}$$

In the low Er^{3+}-densities (near $10^{26}\ m^3$), the occupation factors can not be effected from the temperature variation. The long range temperature variations can be changed the emission and absorption coefficient, but in this study, the temperature range is not wide. It is only 15 °C. From this point of view, we do not consider the occupation factors for erbium. This study is confined by inserting the occupation factors of ytterbium.

The absorption coefficient α_a due to the Er^{3+} and Yb^{3+} ions in the single mode core and is given by the following equation:

$$\alpha_a = \Gamma_p[\sigma'_{pa}(N_{Yb} - N_6) - \sigma'_{pe}N_6] + \Gamma_p[\sigma_{pa}(N_{Er} - N_2) - \sigma_{pe}N_2] \tag{19}$$

where Γ_p and Γ_s are the proportions of the pump power and signal power (Er), the signal power S is given by the following equation:

$$\frac{dS(z,\nu_i)}{dz} = -S(z,\nu_i)\iint_A \frac{[N_{Er}\sigma_{sa} - N_2(\sigma_{sa}+\sigma_{se})]}{\psi_s(x,y)dxdy - \alpha S(z,\nu_i)} \tag{20}$$

where $S(z,\nu_i)$ is the signal power of the frequency $\nu_i$at the z position of the co-doped fiber (CDF), α is the background loss at the signal wavelength, and $\psi_s(x,y)$ is the spatial distribution of the signal light determined by the beam shape.

3. Gain and noise figure

The signal gain G is

$$G = \exp\left(\int_0^L g(z)dz\right), \tag{21}$$

where $g(z)$ is the gain for the Er transition per unit length, which depends on the position of z, and is given by

$$g(z) = \Gamma_s[N_2\sigma_{se} - \sigma_{sa}(N_{Er} - N_2)] \tag{22}$$

The basic optical methods that used for measuring noise figure (NF) are source subtraction technique, polarization nulling and time-domain extinction (plus method) [23]. Differences in these methods are in the ways the source spontaneous emission (SSE) is accounted for and how the noise and gain are measured. The above optical methods of NF measurement depend on the measurement of the amplified spontaneous emission (ASE) density. Therefore, care should obtain accurate amplifier noise figure.

The optical source subtraction method is used for straightforward characterization of the gain and noise figure performance of optical amplifiers. The SSE is measured and subtracted from the total noise emitted by amplifier to obtain the true ASE. The noise figure is calculated according to the following equation:

$$NF = \frac{1}{G} + \frac{P_{ASE}}{GhvB_0} - \frac{P_{SSE}}{hvB_0} \tag{23}$$

where $\frac{1}{G}$ is the shot noise, v is the signal frequency, and B_0 is the noise bandwidth used to measure the powers P_{ASE} and P_{SSE}. For each signal wavelength, the noise figure is given by [23]:

$$NF(dB) = 10\log_{10}\left[\frac{1}{G} + \frac{P_{ASE}}{GhvB_0} - \frac{P_{SSE}}{hvB_0}\right] \tag{24}$$

4. Numerical results and discussion

Normally rate equations can be solved analytically in steady state and these solutions are substituted into propagation equations to calculate the signal gain and also noise figure. The analytical solution of the temperature-dependent model is preformed together with a standard model for light propagation in erbium-doped fiber amplifier, including the ASE from the lasing level [24]. The results of numerical simulation are done by Mathematica Software and using Intel visual Fortran Complier.

The parameters used as the starting point in the calculation are shown in Table 1.

The calculated signal gain and noise figure at temperatures of 25 and 40 °C for different pumping powers at 1060 nm are shown in Figs. 4 and 5, respectively. In Fig. 4 the fiber of length 0.3 m is selected to obtain the high signal gain and the low noise figure. An input signal power of 1 μW at the signal wave length of 1535 nm is used in the signal gain and noise figure calculations. The pump powers we used at the pump wavelength of 1060 nm are 100 mW and 200 mW. At the small pump power of 100 mW, a signal gain of 33.5 dB at the temperature of 25 °C is obtained from the 0.3 m-long fiber whereas a signal gain of 33.0 dB at the temperature of 40 °C is achieved from the same fiber. In this case, the variation of the signal gain becomes 0.5 dB when the temperature is increased from 25 to 40 °C. At the pump power of 200 mW, the achieved signal gain is near 40.5 dB without influencing from the variation of temperature. An increment of the pump power to 200 mW from 100 mW gives a signal gain of 7–7.5 dB. It is an interesting result that the numerical calculations obtained with respect to the signal gain at the high pump power, 200 mW, are approximately independent of the variation of the temperature in the end of fiber (see Fig. 4). Fig. 5 shows the noise figure as a function of amplifier length of 0.3 m for a fixed signal power of 1 μW at the signal wavelength of 1535 nm. The plot is results for several pump power applications, i.e., 100 and 200 mW, as well as for temperature values of 25 and 40 °C. At low pump power, 100 mW, the noise figure increases up to 3.39 dB from 3.34 dB when the temperature is increased to 40 °C from 25 °C. At high pump power, 200 mW, the noise figure increases up to 3.76 dB from 3.65 dB when the temperature is increased to 40 °C from 25 °C. It is clear that the variation of noise figure at low pump power is smaller than that of high pump power when the temperature is increased to 40 from 25 °C. Moreover, it is an interesting result that the signal gain at high pump power does not influence from the variation of temperature whereas the noise figure shows a poor effect depend on the variation of temperature.

We also investigated the influence of several signal powers on the signal gain at temperatures of 25 and 40 °C. At the fixed pump power of 200 mW, the signal gain versus the amplifier length at three different pumping powers for signal of wavelength 1535 nm is shown in Fig. 6 at the temperature of 25 °C and in Fig. 7 at the temperature of 40 °C. When increasing the signal powers from 1 to 100 μW. It can be noticed that the decrease of the gain with increasing signal input power is simply due to saturation

Table 1
The numerical parameters used in the model.

Yb concentration	$N_{Yb} = 1.2 \times 10^{27}$ m^{-3}
Er concentration	$N_{Er} = 1.0 \times 10^{26}$ m^{-3}
The core radius	2.5 μm
Doped radius	2 μm
Numerical aperture (NA)	0.25
The proportion of the pump and signal power of Er	$\Gamma_s = \Gamma_p = 1$
The noise bandwidth	$B_0 = 1$ nm
The pump stimulated absorption cross-section of Yb	$\sigma'_{pa} = 2.0 \times 10^{-24}$ m^2
The pump stimulated emission cross-section of Yb	$\sigma'_{pe} = 1.5 \times 10^{-24}$ m^2
The pump stimulated absorption cross-section of Er	$\sigma_{pa} = 5.5 \times 10^{-25}$ m^2
The pump stimulated emission cross-section of Er	$\sigma_{pe} = 5 \times 10^{-25}$ m^2
The signal stimulated absorption cross-section of Er for 1535 nm	$\sigma_{sa} = 5 \times 10^{-25}$ m^2
The signal stimulated emission cross-section of Er for 1535 nm	$\sigma_{se} = 6.6 \times 10^{-25}$ m^2
The signal stimulated emission cross-section of Yb; for 1060 nm	$\sigma'_{se} = 2.6 \times 10^{-25}$ m^2
The transfer coefficient	$K = 3 \times 10^{-20}$ m^3 s^{-1}
For the laser transition $f_a = 0.0168$, $f_b = 0.67$, $f'_a = 0.72$ and $f'_b = 0.33$ at T = 25 °C and $f_a = 0.0192$, $f_b = 0.65$, $f'_a = 0.70$ and $f'_b = 0.35$ at $T = 40$ °C	

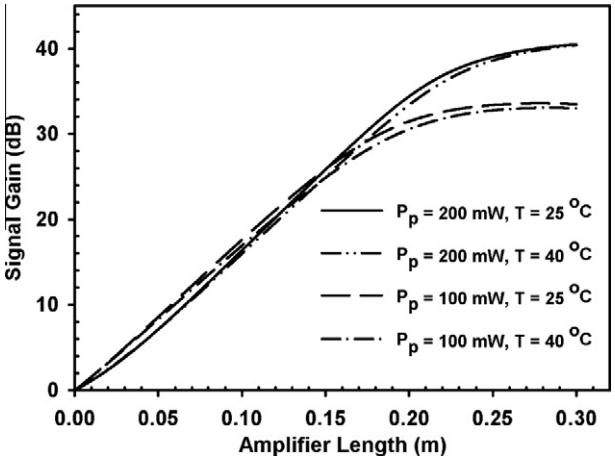

Fig. 4. The signal gain (dB) via amplifier length. $P_s = 1$ μW at 1535 nm signal wavelength.

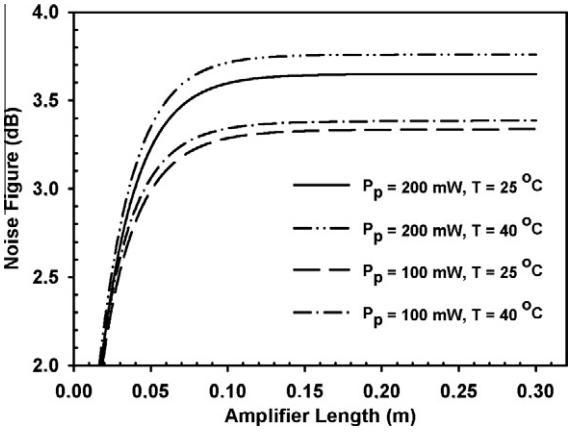

Fig. 5. The noise figure (dB) via amplifier length. $P_s = 1$ μW at 1535 nm signal wavelength.

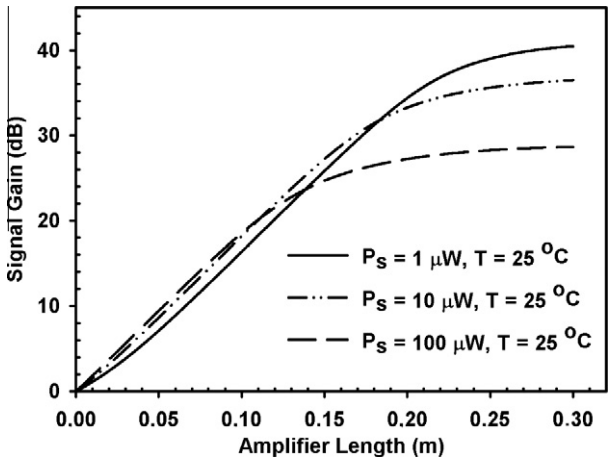

Fig. 6. The variation of signal gain according to the amplifier length at three different signal powers for signal of wavelength 1535 nm. The pump power and temperature are fixed at 200 mW and 25 °C, respectively.

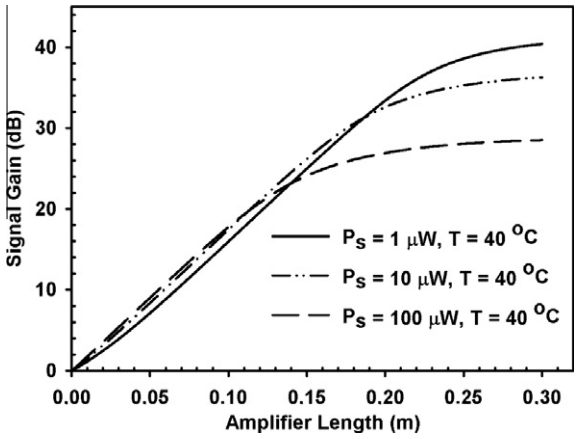

Fig. 7. The variation of signal gain according to the amplifier length at three different signal powers for signal of wavelength 1535 nm. The pump power and temperature are fixed at 200 mW and 40 °C, respectively.

effects in the amplifier (i.e. the signal power becomes comparable to the pump power and acts as a negative pump reducing population inversion). The above investigation has also been studied at the same temperatures at another fixed pump power of 100 mW

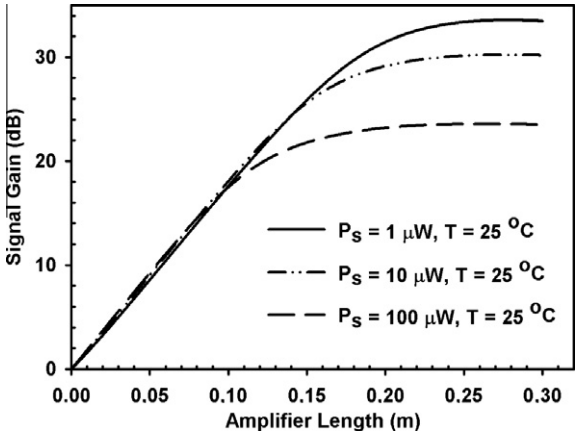

Fig. 8. The variation of signal gain according to the amplifier length at three different signal powers for signal of wavelength 1535 nm. The pump power and temperature are fixed at 100 mW and 25 °C, respectively.

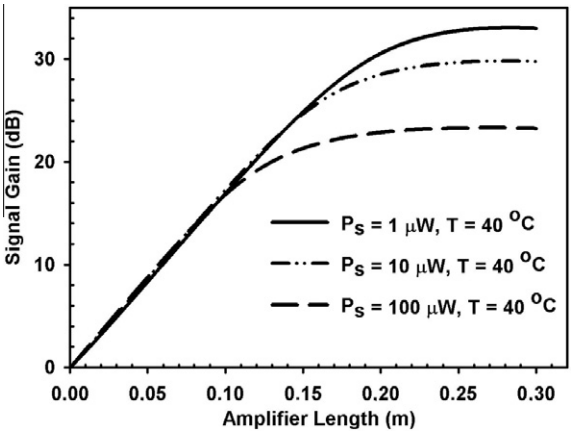

Fig. 9. The variation of signal gain according to the amplifier length at three different signal powers for signal of wavelength 1535 nm. The pump power and temperature are fixed at 100 mW and 40 °C, respectively.

Table 2
Numerical results with respect to the temperatures of 25 and 40 °C.

Pump power (mW)	Signal power (μW)	Signal gain (dB)	
		25 °C	40 °C
200	1	40.5	40.5
	10	36.5	36.3
	100	28.7	28.5
100	1	33.5	33.0
	10	30.2	29.8
	100	23.5	23.3

and presented in Figs. 8 and 9. The same conclusion is achieved when the three signal powers used; 1, 10, and 100 μW. Table 2 presents the effect of temperature on the signal gain at two different pump powers and at three different pumping powers. It can be seen from Table 2 is that when pumping at 100 mW pump power, it is the smallest input signal (1 μW) which suffers the largest gain variation (−0.5 dB) with a temperature change from 25 to 40 °C, and for higher input signals the variation is progressively reduced. On the contrary, at 200 mW pump power it is the highest input signal which experiences the largest gain variation (−0.2 dB).

The temperature dependence of the Yb–Er-codoped fiber amplifier performance is investigated by plotting gain and NF versus temperature in Figs. 10 and 11, respectively. In Fig. 10 it can be seen that in the pump power of 100 mW, when the temperature increases to 40 °C from 25 °C, the gain value decreases moderately

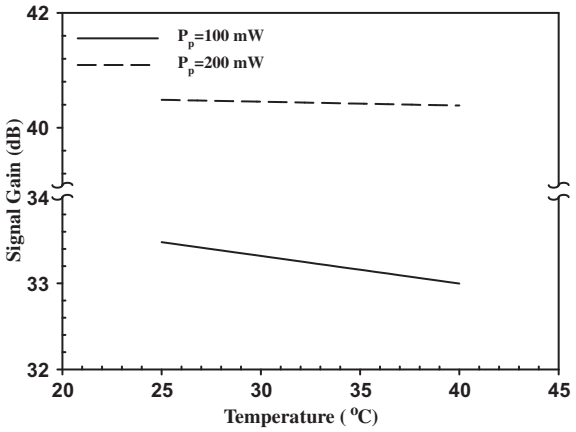

Fig. 10. The variation of gain versus temperature in two different pump powers.

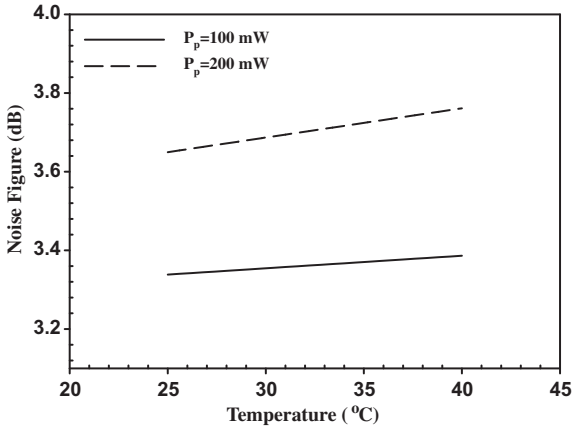

Fig. 11. The variation of NF versus temperature in two different pump powers.

to 33.5 dB from 33.0 dB. In the pump power of 200 mW, there is no variation on the gain versus temperature. We concluded that when operating the Yb–Er-codoped fiber amplifier at low pump power, the amplifier performance is not desirable situation. Fig. 11 shows that the NF increases with increasing temperature. In the high pump powers, the NF depends much more on temperature.

5. Conclusion

We have used the temperature-dependent model for Yb^{3+}–Er^{3+}-codoped fiber amplifier (EYDFA) and illustrated the strategy with results for the gain and noise figure using appropriate fiber and energy transfer parameters. These results show how an EYDFA performs as a function of temperature, how small signal powers influence the performance of the amplifier, and what the requirements are to increase the signal gain and to reduce the noise figure. The temperature-dependent calculations are performed at the temperatures of 25 and 40 °C. The pumping powers are selected as 100 and 200 mW at the pump wavelength of 1060 nm. The signal gain and noise figure of EYDFA with three different signal powers are reported. Using a 0.3 m-long erbium/ytterbium co-doped fiber (EYDF) in a single-pass configuration, 40.5 dB signal gain and the corresponding noise figure of 3.65 dB for a small signal power, 1 μW, are achieved at 1060 nm pump power of 200 mW at the temperature of 25 °C.

References

[1] E. Desurvire, Erbium Doped Fiber Amplifier, John Wiley and Sons Inc., New York, 1994.
[2] C.C. Ye, P.R. Morkel, E.R. Taylor, D.N. Payne, Direct observation of cooperative upconversion mechanisms in erbium-doped fiber amplifiers, Presented at ECOC 93, Montreux, Sep. 1993.
[3] B.-H. Choi, H.-H. Park, M.-J. Chu, IEEE Journal of Quantum Electronics 39 (10) (2003) 1272.
[4] C. Berkdemir, S. Özsoy, The temperature dependent performance analysis of EDFAs pumped at 1480 nm: a more accurate propagation equation, Optics Express 13 (13) (2005) 5179–5185.
[5] Cheng Cheng, Min Xiao, Optimization of an erbium-doped fiber amplifier with radial effects, Optics Communications 254 (4-6) (2005) 215–222.
[6] C. Berkdemir, S. Özsoy, An investigation on the temperature dependence of the relative population inversion and the gain in EDFAs by the modified rate equations, Optics Communications 254 (4–6) (2005) 248–255.
[7] S.W. Harun, H. Ahmad, Gain and noise figure improvements in double-pass S-band EDFA, Optics & Laser Technology 39 (2007) 935–938.
[8] Ali H. El-Astal, Abdel Hakeim M. Husein, Majdi S. Hamada, The temperature dependency of EDFAs in the 1480 nm pumping configuration, Optics Communications 278 (1) (2007) 71–76.
[9] S.W. Harun, H.A. Abdul-Rashid, S.Z. Muhd-Yassin, M.K. Abd-Rahman, K.K. Jayapalan, H. Ahmad, 37.2 dB small-signal gain from Er/Yb Co-doped fiber amplifier with 20 mW pump power, Optics & Laser Technology 40 (2008) 88–91.
[10] J. Zhang, S. Dai, G. Wang, H. Sun, L. Zhang, L. Hu, Fabrication and emission properties of Er^{3+}/Yb^{3+} codoped tellurite glass fiber for broadband optical amplification, Journal of Luminescence 115 (2005) 45–52.
[11] Z. Meng, K. Nagamatsu, M. Higashihata, Y. Nakata, T. Okadab, Y. Kubota, N. Nishimura, T. Teshima, S. Buddhudu, Energy transfer mechanism in Yb^{3+}:Er^{3+}-ZBLAN: macro- and micro-parameters, Journal of Luminescence 106 (2004) 187–194.
[12] G. Lakshminarayana, Jianrong Qiu, M.G. Brik, G.A. Kumar, I.V. Kityk, Spectral analysis of Er^{3+}-, Er^{3+}/Yb^{3+}- and $Er^{3+}/Tm^{3+}/Yb^{3+}$-doped TeO_2–ZnO–WO_3–TiO_2–NaO_2 glasse, Journal of Physics: Condensed Matter 20 (2008) 375101.
[13] W.L. Barnes, S.B. Pool, J.E. Townsend, L. Reekie, D.J. Taylor, D.N. Payne, Er^{3+}–Yb^{3+} doped fiber laser, Journal of Lightwave Technology 7 (10) (1989) 1461–1465.
[14] Y. Liu, C. Wang, Y. Lu, Gain characteristic of a ytterbium doped fiber amplifier at 1064 nm, in: Proc. Of Spie, vol. 6344, 63340L, 2006.
[15] R. Paschotta, J. Nillisson, A.C. Tropper, D.C. Hanna, Ytterbium doped fiber amplifier, IEEE Journal of Quantum Electronics 33 (7) (1997) 1049–1056.
[16] F. Di Pasquale, M. Federighi, Improved gain characteristics in high-concentration Er^{3+}/Yb^{3+} codoped glass waveguide amplifiers, IEEE Journal of Quantum Electronics 30 (9) (1994) 2127–2131.
[17] D.S. Knowles, H.P. Jenssen, Upperconversion in erbium and its dependence on energy migration, OSA Technical Digest Series 11 (1993) 310–311.
[18] T. Georges, E. Delevaque, M. Monerie, P. Lamouler, J.F. Bayon, Pair induced quenching in erbium doped silicate fibers, in: Opt. Amp. Tech., vol. 17, Digest Optical Society of America, 1992, pp. 71–74.
[19] O. Lumholt, T. Rasmussen, A. Bjarklev, Modeling of extremely high concentration erbium-doped silica waveguides, Electron. Lett. 29 (1993) 495–496.
[20] M. Karasek, Optimum design of Er^{3+}/Yb^{3+} codoped fibers for large signal high-pump-power applications, IEEE Journal of Quantum Electronics 33 (10) (1997) 1699–1705.
[21] T.Y. Fan, Optimizing the efficiency and stored energy in quasi three-level lasers, IEEE Journal of Quantum Electronics 28 (12) (1992) 2692–2697.
[22] B. Majaron, H. Lukac, M. Copic, Population dynamics in Yb:Er: phosphate glass under neodymium laser pumping, IEEE Journal of Quantum Electronics 31 (2) (1995) 301–308.
[23] S. Pool, Noise figure measurement in optical fiber amplifiers, NIST Special Publication 846 (1994) 1–6.
[24] B. Pedersen, A. Bjarklev, J.H. Povlsen, K. Dybdal, C.C. Larsen, The design of erbium-doped fiber amplifier, Journal of Lightwave Technology 9 (1991) 1105–1112.

Abdel Hakem M. Husein was born in 1965, Gaza, Palestine. In 1992, he got his B.Sc. in Physics from the Islamic university of Gaza. In 1999 did his M.Phil degree in Laser Optoacoustics from Keele University, UK. In 2009 his Ph.D. research was in fiber optics and communications from the joint program between Al-aqsa University/Gaza and Ein Shams University/Cairo. He published refereed papers and participated in conferences.

Prof. Ali H. El-Astal was born in 1964, Gaza, Palestine. In 1986 he got his B.Sc from UAE University and the M.Sc. (1991) in optoelectronics and optical information processing and Ph.D. (1995) in laser physics from the Queen's University of Belfast, UK. From 1996 until now, he has been working at department of physics, Al-Aqsa University, Gaza, Palestine. He published various refereed papers on laser physics and other related topics and participated in many conferences.

Fady I. El-Nahal received his B.Sc. degree in electrical and electronic engineering in 1996 from Alfateh University and his M.Phil. and Ph.D. degrees from the University of Cambridge in 2000 and 2004 respectively. He is currently with the Department of Electrical & Computer Engineering, The Islamic University of Gaza. His research activities include optoelectronics, optical communications and wavelength routing in optical networks. Fady is a Fellow of the Cambridge Overseas Trust and the president of the Oxford and Cambridge Society of Palestine.